International Journal of Precision Engineering and Manufacturing (2022) 23:701–710
https://doi.org/10.1007/s12541-022-00653-y

Online ISSN 2005-4602
Print ISSN 2234-7593

REGULAR PAPER

A Dual Difference Method for Identification of the Inherent Spindle Axis Parallelism Errors of Machine Tools

Seung-Han Yang[1] · **Kwang-Il Lee**[2]

Received: 6 January 2022 / Revised: 20 February 2022 / Accepted: 30 March 2022 / Published online: 2 May 2022

Abstract

It is essential to identify spindle axis parallelism errors because such errors trigger volumetric errors when tools of different lengths are used. However, only a few works have addressed this issue. Thus, we identified the inherent spindle axis parallelism errors of machine tools relative to the end-point reference straight line of the Z-axis (according to ISO 230-1) using a dual difference method. Here, "inherent" refers to parallelism errors of the spindle axis that are not affected by the geometric errors of other axes controlled during the measurements, and "dual difference" refers to the difference in the differences of measuring data. The dual difference method uses two pairs of circular tests performed with the aid of a double ball-bar (DBB); the tool lengths differ during each test and the DBB set-up is shared by the pairs. Parallelism errors are then identified based on the dual differences within and between the two pairs. Experimentally, the maximum peak-to-valley (PV) values were 54.5 and 48.7 μm for differences in radial deviations within the two pairs when the parallelism errors were not compensated. After tool-center-point compensation by the identified errors, the PV values improved to 8.0 and 9.2 μm, respectively, showing that compensation was successful. In addition, the concentricity of two holes machined using tools of different lengths improved from 31.2 μm without compensation to 15.9 μm with compensation, further demonstrating the effectiveness of the method.

Keywords Circular test · Dual difference method · Machine tools · Parallelism errors · Spindle axis

List of Symbols

l_i	Offset ($i=1, \ldots, 3$), mm.
n_i	Number of samples during the i-th circular test ($i=1, \ldots, 4$).
s_{ij}	Squareness error of the j axis around the i direction ($i, j=x, y, z$), rad.
p_{xs}, p_{ys}	Parallelism errors of the spindle axis around the x and y directions, respectively, rad.
δ_{ij}	Positional error of the j axis in the i direction ($i, j=x, y, z$), mm.
ε_{ij}	Angular error of the j axis around the i direction ($i, j=x, y, z$), rad.
θ_j	Rotation angle during the circular test ($j=1, \ldots, n_i$), rad.
R	Nominal length of the double ball-bar, mm.
ΔR_{ij}	j- th measured radial deviation during the i-th circular test ($i=1, \ldots, 4$; $j=1, \ldots, n_i$), mm.
(w_{xi}, w_{yi}, w_{zi})	Set-up errors of a ball on a workpiece table in the x, y, and z directions, respectively, during the i-th circular test, ($i=1, \ldots, 4$), mm.
$(0, 0, t_i)$	Nominal coordinate of a ball at the tool nose in the spindle coordinate system $\{\boldsymbol{S}\}$ during the i-th circular test, ($i=1, \ldots, 4$), mm.
$(0, 0, h_i)$	Nominal coordinate of a ball on a workpiece table in the workpiece coordinate system $\{\boldsymbol{W}\}$ during the i-th circular test, ($i=1, \ldots, 4$), mm.

✉ Kwang-Il Lee
kilee@kiu.kr

Seung-Han Yang
syang@knu.ac.kr

[1] School of Mechanical Engineering, Kyungpook National University, 80, Daehak-ro, Buk-gu, Daegu 41566, Republic of Korea

[2] School of Mechanical and Automotive Engineering, Kyungil University, 50, Gamasil-gil, Hayang-eup, Gyeongsan-si, Gyeongbuk 38428, Republic of Korea

(x, y, z)	Nominal commands of the X, Y, and Z axes, respectively, mm.
$\{i\}$	Coordinate system of axis i, ($i = X, Y, Z$).
$\{R\}$, $\{W\}$, $\{S\}$, $\{t\}$	Coordinate systems of the reference, workpiece, spindle, and tool, respectively.
$\boldsymbol{\tau}_i^j$	4×4 Homogeneous transformation matrix from the j coordinate system to the i coordinate system.

1 Introduction

To improve machine tool volumetric accuracy, it is important to measure and compensate for geometric errors caused by structural elements, which in turn cause kinematic errors, and for directly measured stiffness, gravity, and thermal errors [1]. Geometric errors can be divided into position-independent geometric errors (PIGEs) and position-dependent geometric errors (PDGEs) under no-load or quasi-static conditions [2]. The volumetric errors of three-axis machine tools are modeled using 23 geometric errors, including 6 PDGEs for each linear axis, 3 PIGEs between the linear axes, and 2 parallelism errors of the spindle axis [3, 4].

Both direct and indirect methods can be used to measure geometric errors [5, 6]. The direct methods involve single-axis control during measurement, while the indirect methods involve the control of more than one axis. Laser interferometry is widely used to measure the PDGEs of linear axes [7] by determining measurement points to compensate for the geometric errors [8] and using invariant approaches to replace the Abbe and Bryan principles [9]. A double ball-bar (DBB) can also be applied to identify kinematic errors using circular tests [10] and geometric errors by developing a reconfigurable mechanism model [11]. Additionally, PIGEs are identified by diagonal displacement tests using a laser interferometer [12] and a DBB with an extension fixture [13]. In summary [14], the PDGEs and PIGEs of machine tools are measurable in various ways and can be compensated via computerized numerical control to improve volumetric accuracy. However, only a few methods are available for identification of parallelism errors in a spindle axis. A mandrel method identifies parallelism errors by sequentially measuring deviations of the test mandrel in the X- and Y-directions, using a dial gauge with a moving Z-axis as depicted in G12 of ISO 10791-1:2015 [15]. However, the identified errors are affected by Z-axis PDGEs, and it is difficult to apply the method to the full travel of the Z-axis in machines with a vertical spindle, due to collisions between the mandrel and workpiece table [16]. A linear displacement sensor is used to measure a test sphere at different positions in 10.1.4.4 of ISO 230-1:2012 [3], and a DBB

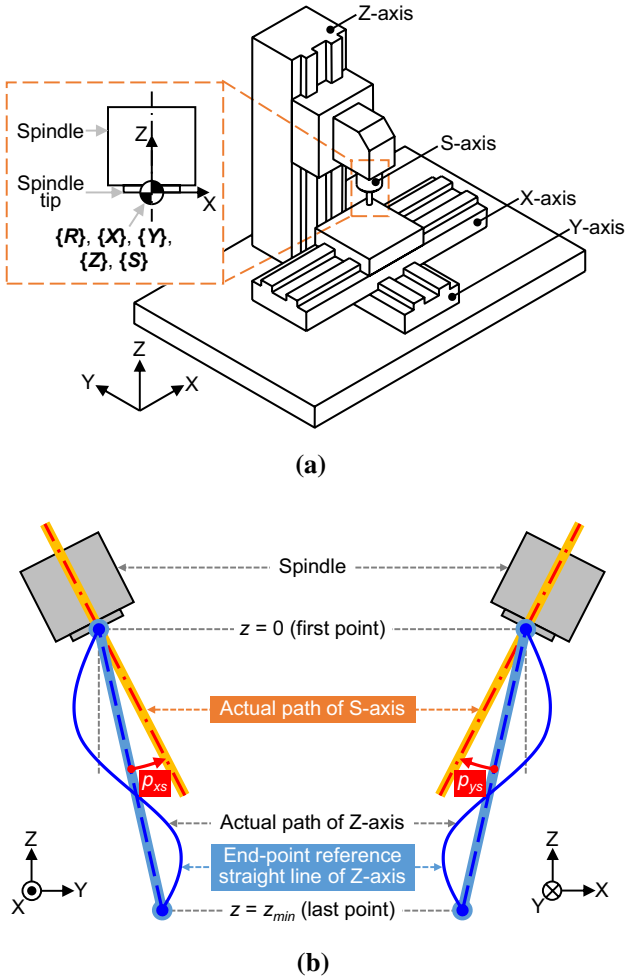

Fig. 1 Experimental machine tool and end-point reference straight line of the Z-axis. **a** Kinematic structure of the machine tool. **b** Parallelism error in the YZ and ZX planes

method featuring circular tests that employ tools of different lengths [17, 18] has been used to identify parallelism errors by enlarging the differences between tool lengths; however, such measurements are also affected by Z-axis PDGEs. In the case of five-axis machine tools, squareness errors, interchangeable with parallelism errors, are used to describe the spindle axis relative to a rotary axis; squareness errors can be identified using PIGEs of other axes with DBB measurements by simultaneous control of the linear and rotary axes [1, 19]. Thus, identified squareness errors are affected by the PDGEs of linear and rotary axes. The limitations arise because parallelism errors are representative angular deviations of the spindle axis relative to the Z-axis. Thus, it is essential to define the reference straight line of the Z-axis prior to parallelism error identification. However, the need to establish the reference line increases the cost of the test; a simpler and cheaper method is required.

In general, geometric errors are calculated as the sum of sensitivity coefficients multiplied by measured data [20]. Various factors contribute to the uncertainties of measured data [21]; the uncertainties of measured geometric errors are estimated by error budgeting [22]. On the contrary, the sensitivity coefficients are affected mainly by the measuring paths [23]. Thus, the root-sum-squared (RSS) values of sensitivity coefficients are used to determine measurement conditions under the assumption that the uncertainties of measured data are equal.

Here, we identified inherent parallelism errors of the machine tool spindle axis relative to the end-point reference straight line of the Z-axis (the line of ISO 230-1) using a dual difference method. This requires only two pairs of sequential circular tests, using a DBB with extension bars; thus, the method is simple and cost-effective. Section 2 introduces the dual difference method, including the measuring paths and the algorithm that identifies the parallelism errors. In Sect. 3, these errors are experimentally identified by the dual difference method, with analysis of the RSSs of the sensitivity coefficients. The identified errors are also validated by evaluating the positional deviations and concentricity of two holes machined using tools of different lengths, without and with error compensation. Section 4 provides the conclusion and summarizes the principal findings.

2 Dual Difference Method

2.1 Geometric Errors and Error Synthesis Model

The kinematic structure of the machine tool with a vertical spindle used in this study is shown in Fig. 1a, together with the reference coordinate system, as well as the linear axes and the spindle axis at the initial position of the spindle tip. Geometrically, spindle axis parallelism errors are representative angular deviations relative to the reference straight line of the Z-axis in the YZ and ZX planes, as shown in Fig. 1b. Three methods are commonly used to define the reference straight line for the Z-axis: the minimum zone, least-squares, and end-point methods [3]. We used the end-point method to identify inherent parallelism errors.

Volumetric errors $\boldsymbol{\tau}_W^t$, as functions of the nominal coordinates (x, y, z), and geometric errors are derived using the homogeneous transformation matrix method [24] of Eq. (1). Here, $(0, 0, t_i)$ and $(0, 0, h_i)$ refer to the nominal position of a ball at the tool nose in coordinate system $\{\boldsymbol{S}\}$ and the nominal position of a ball on the workpiece table in coordinate system $\{\boldsymbol{X}\}$, respectively, during DBB measurements. The set-up errors (w_{xi}, w_{yi}, w_{zi}), which are caused by geometric errors and thus do not change during measurements, are used to describe the actual position of the ball on the workpiece table in the coordinate system $\{\boldsymbol{X}\}$. It is not necessary to model the position of a ball at the tool nose using set-up errors, because it assumed that the ball is positioned on the spindle axis using adjustment fixtures [25].

(Workpiece branch).

$$\boldsymbol{\tau}_R^Y = \begin{bmatrix} 1 & -\varepsilon_{zy} & \varepsilon_{yy} & \delta_{xy} \\ \varepsilon_{zy} & 1 & -\varepsilon_{xy} & -y+\delta_{yy} \\ -\varepsilon_{yy} & \varepsilon_{xy} & 1 & \delta_{zy} \\ 0 & 0 & 0 & 1 \end{bmatrix},$$

$$\boldsymbol{\tau}_Y^X = \begin{bmatrix} 1 & -s_{zx}-\varepsilon_{zx} & \varepsilon_{yx} & -x+\delta_{xx} \\ s_{zx}+\varepsilon_{zx} & 1 & -\varepsilon_{xx} & -xs_{zx}+\delta_{yx} \\ -\varepsilon_{yx} & \varepsilon_{xx} & 1 & \delta_{zx} \\ 0 & 0 & 0 & 1 \end{bmatrix},$$

$$\boldsymbol{\tau}_X^W = \begin{bmatrix} 1 & 0 & 0 & w_{xi} \\ 0 & 1 & 0 & w_{yi} \\ 0 & 0 & 1 & h_i+w_{zi} \\ 0 & 0 & 0 & 1 \end{bmatrix},$$

(Tool branch).

$$\boldsymbol{\tau}_R^Z = \begin{bmatrix} 1 & -\varepsilon_{zz} & s_{yz}+\varepsilon_{yz} & zs_{yz}+\delta_{xz} \\ \varepsilon_{zz} & 1 & -s_{xz}-\varepsilon_{xz} & -zs_{xz}+\delta_{yz} \\ -s_{yz}-\varepsilon_{yz} & s_{xz}+\varepsilon_{xz} & 1 & z+\delta_{zz} \\ 0 & 0 & 0 & 1 \end{bmatrix},$$

$$\boldsymbol{\tau}_Z^S = \begin{bmatrix} 1 & 0 & p_{ys} & 0 \\ 0 & 1 & -p_{xs} & 0 \\ -p_{ys} & p_{xs} & 1 & 0 \\ 0 & 0 & 0 & 1 \end{bmatrix},$$

$$\boldsymbol{\tau}_S^t = \begin{bmatrix} 0 \\ 0 \\ t_i \\ 1 \end{bmatrix},$$

$$\boldsymbol{\tau}_W^t = \left(\boldsymbol{\tau}_R^Y \boldsymbol{\tau}_Y^X \boldsymbol{\tau}_X^W\right)^{-1} \boldsymbol{\tau}_R^Z \boldsymbol{\tau}_Z^S \boldsymbol{\tau}_S^t$$

$$= \begin{bmatrix} x+y\left(\varepsilon_{zx}+\varepsilon_{zy}+s_{zx}\right)+z\left(-\varepsilon_{yx}-\varepsilon_{yy}+s_{yz}\right)-\delta_{xx}-\delta_{xy}+\delta_{xz}+t_i\left(-\varepsilon_{yx}-\varepsilon_{yy}+\varepsilon_{yz}+s_{yz}+p_{ys}\right)-w_{xi} \\ -x\varepsilon_{zx}+y+z\left(\varepsilon_{xx}+\varepsilon_{xy}-s_{xz}\right)-\delta_{yx}-\delta_{yy}+\delta_{yz}+t_i\left(\varepsilon_{xx}+\varepsilon_{xy}-\varepsilon_{xz}-s_{xz}-p_{xs}\right)-w_{yi} \\ x\varepsilon_{yx}-y\left(\varepsilon_{xx}+\varepsilon_{xy}\right)+z-h_i+t_i-\delta_{zx}-\delta_{zy}+\delta_{zz}-w_{zi} \\ 1 \end{bmatrix} \quad (1)$$

2.2 Measuring Paths and Identification Algorithm

The dual difference method features two pairs of circular tests; the results identify spindle axis parallelism errors relative to the end-point reference straight line of the Z-axis (Fig. 2). The first and third circular tests (Fig. 2a, c) are performed at the first point ($z=0$) of the Z-axis, and the second and fourth tests (Fig. 2b, d) are performed at the last point ($z=z_{min}=l_2$). The tool length t_i and workpiece height h_i are summarized in Table 1. Note that the offset l_2 is equal to z_{min}; the DBB measurements are thus performed at the first and last points of the Z-axis when establishing the end-point reference straight line. Note that the set-up ball on the workpiece table is shared by each pair; this cancels set-up errors by the difference. Thus, the set-up errors of a ball on the workpiece table are the same within each pair; $(w_{x1}, w_{y1}, w_{z1})=(w_{x2}, w_{y2}, w_{z2})$, $(w_{x3}, w_{y3}, w_{z3})=(w_{x4}, w_{y4}, w_{z4})$.

Table 1 Signed tool length t_i and workpiece height h_i of measuring paths

Signed tool length	Value	Workpiece height	Value
t_1	l_1+l_2	h_1	l_1+l_2
t_2	l_1	h_2	l_1+l_2
t_3	$l_1+l_2+l_3$	h_3	$l_1+l_2+l_3$
t_4	l_1+l_3	h_4	$l_1+l_2+l_3$

The linearized relationships between the radial deviations ΔR_{ij}, and the geometric and set-up errors are shown in Eq. (2), which uses Eq. (1):

$$\begin{aligned}\Delta R_{ij} = {} & \left\{\delta_{xx}+\delta_{xy}-\delta_{xz}+t_i\left(-\varepsilon_{yz}-p_{ys}\right)+h_i\left(\varepsilon_{yx}+\varepsilon_{yy}-s_{yz}\right)+w_{xi}\right\}\cos\theta_j \\ & +\left\{\delta_{yx}+\delta_{yy}-\delta_{yz}+t_i\left(\varepsilon_{xz}+p_{xs}\right)+h_i\left(-\varepsilon_{xx}-\varepsilon_{xy}+s_{xz}\right)+w_{yi}\right\}\sin\theta_j+\frac{R}{2}\left(\varepsilon_{zy}+s_{zx}\right)\sin 2\theta_j\end{aligned} \tag{2}$$

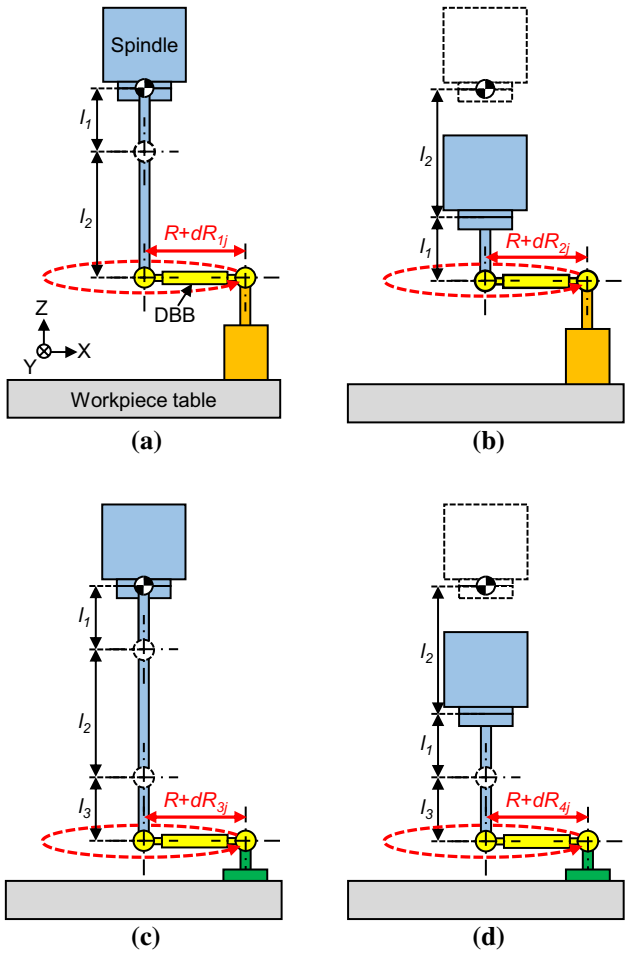

Fig. 2 Circular test paths of the dual difference method for identification of parallelism errors. **a** 1st path. **b** 2nd path. **c** 3rd path. **d** 4th path

Equation (2) reveals that the radial deviations (ΔR_{ij} values) of a circular test are affected by geometric and set-up errors with sensitivity coefficients of $\cos\theta_j$, $\sin\theta_j$, and $\sin 2\theta_j$, respectively. The mandrel method [15] measures radial deviations at $\theta_j=0$ and $\pi/2$ when $R=0$. Thus, it is difficult to identify inherent parallelism errors using a circular test and/or a mandrel method, because both approaches require pre-measures of the geometric errors of the linear axes, as well as pre-measures of the set-up errors. Importantly, the effects of set-up errors on identified parallelism errors can be eliminated by comparing measured deviations at different Z-axis positions [16] and by sharing the circular test set-up among different tool lengths [17]. Nevertheless, these approaches are affected by Z-axis PDGEs and thus do not reliably identify inherent parallelism errors.

When identifying inherent parallelism errors using the dual difference method, all PDGEs at the first point of the Z-axis are assumed to be zero; the straightness errors δ_{xz}, δ_{yz} are also zero at the last point, given the definition of the end-point reference straight line of the Z-axis. The differences within pairs are affected by the angular errors ε_{xz} and ε_{yz} at the last point of the Z-axis, and the parallelism errors p_{xs} and p_{ys} [Eq. (3)]. Note that the set-up errors (w_{xi}, w_{yi}, w_{zi}) do not affect the differences because these errors are cancelled when the pairs are set-up ($i=1$ and 2, $i=3$ and 4). Finally, as shown in Eq. (4), the parallelism errors are derived using the dual difference, i.e., the difference of the differences of Eq. (3), and then identified analytically when the circular tests use full circles ($\sum_{j=1}^{n_i}\sin\theta_j=\sum_{j=1}^{n_i}\cos\theta_j=0$) with equal numbers of samples ($n_1=n_2=n_3=n_4$).

$$\begin{aligned}&\left(-l_1\,\varepsilon_{yz}\Big|_{z=z_{\min}}+l_2p_{ys}\right)\cos\theta_j+\left(l_1\,\varepsilon_{xz}\Big|_{z=z_{\min}}-l_2p_{xs}\right)\sin\theta_j=\Delta R_{2j}-\Delta R_{1j}\\&\left\{-\left(l_1+l_3\right)\varepsilon_{yz}\Big|_{z=z_{\min}}+l_2p_{ys}\right\}\cos\theta_j+\left\{\left(l_1+l_3\right)\varepsilon_{xz}\Big|_{z=z_{\min}}-l_2p_{xs}\right\}\sin\theta_j=\Delta R_{4j}-\Delta R_{3j}\end{aligned}\tag{3}$$

$$\begin{bmatrix}p_{xs}\\p_{ys}\end{bmatrix}=\frac{2}{n_i}\begin{bmatrix}-\sum_{j=1}^{n_i}\sin\theta_j\left\{\frac{l_1+l_3}{l_2l_3}\left(\Delta R_{2j}-\Delta R_{1j}\right)-\frac{l_1}{l_2l_3}\left(\Delta R_{4j}-\Delta R_{3j}\right)\right\}\\\sum_{j=1}^{n_i}\cos\theta_j\left\{\frac{l_1+l_3}{l_2l_3}\left(\Delta R_{2j}-\Delta R_{1j}\right)-\frac{l_1}{l_2l_3}\left(\Delta R_{4j}-\Delta R_{3j}\right)\right\}\end{bmatrix}\tag{4}$$

It is essential to explore the effects of measurement conditions on the measurement uncertainties of the parallelism errors identified in Eq. (4). Thus, the measurement uncertainties $U(p_{xs})$ and $U(p_{ys})$ of the parallelism errors in Eq. (4) are derived in Eq. (5), under the assumption that the measurement uncertainties $U(\Delta R_{ij})$ are equal. Here, the RSS values of the sensitivity coefficient consist of offset l_i ($i=1, 2, 3$) and sampling number n_i. It is necessary to identify the measurement conditions that maximally reduce the RSSs of the sensitivity coefficients associated with the reduced measurement uncertainties $U(p_{xs})$ and $U(p_{ys})$, even if the measurement uncertainties $U(\Delta R_{ij})$ do not change. The effects of offset l_i on the RSSs of the sensitivity coefficients are investigated in Sect. 3.

$$\begin{aligned}\begin{bmatrix}U(p_{xs})\\U(p_{ys})\end{bmatrix}&=\text{RSS values of sensitivity coeff.}\times\begin{bmatrix}U(\Delta R_{ij})\\U(\Delta R_{ij})\end{bmatrix}\\&=\frac{2\sqrt{\left(2l_1^2+2l_1l_3+l_3^2\right)}}{l_2l_3\sqrt{n_i}}\times\begin{bmatrix}U(\Delta R_{ij})\\U(\Delta R_{ij})\end{bmatrix}\end{aligned}\tag{5}$$

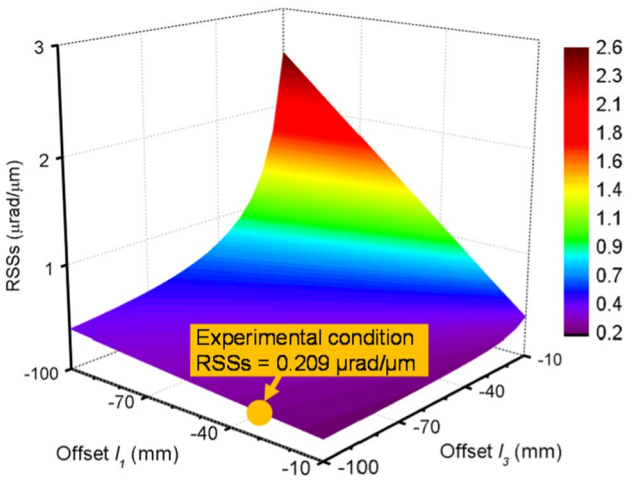

Fig. 3 Root-sum-squared (RSS) values according to offsets l_1 and l_3

3 Experimental

3.1 Parallelism Error Identification

The method in Sect. 2 was applied to the machine tool (SPT-T30; Komatec Co. Ltd, Republic of Korea). A DBB (QC20-W; Renishaw Co. Ltd., UK) was used to identify parallelism errors. The distance between the spindle tip and the workpiece table of the machine tool was 500 mm; the travel range of the Z-axis was [−300, 0] mm. Thus, the mandrel method cannot be applied to this machine tool to identify parallelism errors to the full travel of the Z-axis, due to collisions. It is essential to determine the offset l_i with respect to the distance between the spindle tip and workpiece table, and to define the minimum installable height of a ball on the workpiece table; this is about 70 mm when using the "centre pivot assembly" supplied by the DBB manufacturer. This restricts the offset term $l_1+l_2+l_3$ to −430 mm. Here, offset l_2 is −300 mm (the minimum travel value of the Z-axis); the effects of offsets l_1, l_3 on the RSSs of the sensitivity coefficients are shown in Fig. 3. The RSSs are small for large l_1 and small l_3; l_1 and l_3 were thus set to −30 and −100 mm, respectively.

To identify parallelism errors using the dual difference method, two pairs of sequential circular tests are performed using a DBB with nominal length $R=100$ mm, and nominal offsets $l_1=-30$ mm, $l_2=-300$ mm and $l_3=-100$ mm, as determined above (Fig. 4). The deviations in the offsets during the experiments were not affected by the identified errors, because the deviations cause positional aberration in the Z direction of the ball at the tool nose, and do not affect the radial deviations in the XY plane significantly. Thus, it is not required to measure the tool lengths or offsets during experiments. The overshoot angle is 180° for the DBB measurements; the radial deviations ΔR_{ij} are acquired using DBB software (ver. 5.09.05.03) with $n_i=1{,}504$ samples.

It requires approximately 20 min to complete the circular test measurements with different tool lengths and set-ups. Thus, the proposed dual difference method is easier and cheaper than the existing methods that require a test mandrel, a dial gauge, and pre-measurements of linear axis geometric

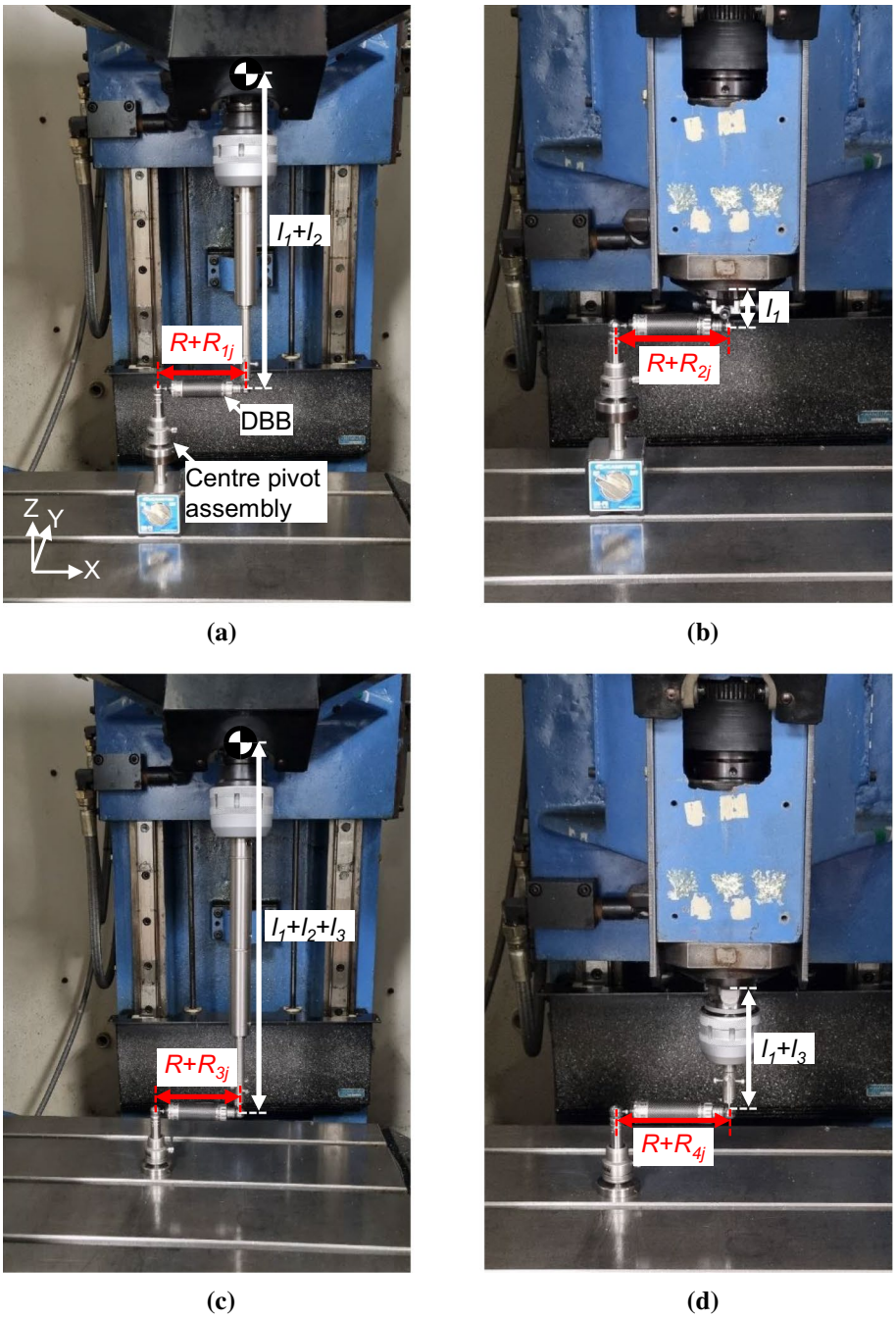

Fig. 4 Experimental set-up for application of the dual difference method. **a** For 1st path. **b** For 2nd path. **c** For 3rd path. **d** For 4th path

errors, for example. The measured ΔR_{ij} show large peak-to-valley (PV) values (Fig. 5a) attributable to parallelism errors, geometric errors of the linear axes, and set-up errors. The parallelism errors are obviously significant because the deviation increases with longer tool lengths ($i = 1$ and 3). The calculated differences within each pair indicate large PVs (Fig. 5b); however, the trends are similar, because the PDGEs of the X and Y axes, as well as the set-up errors, are canceled by the differences. Using the algorithm of Eq. (4), the parallelism errors p_{xs}, p_{ys} were 202.4 and − 74.8 μrad, respectively. The measurements were repeated with compensation for these parallelism errors, both to check the errors and investigate the effects of compensation on the measuring paths. The radial deviations improved significantly after compensation, but they were still affected by the geometric errors of the linear axes and the set-up errors (Fig. 5c). The calculated differences in radial deviations within each pair are shown in Fig. 5d; these reflect only the effects of parallelism errors and Z-axis PDGEs. The PVs improved

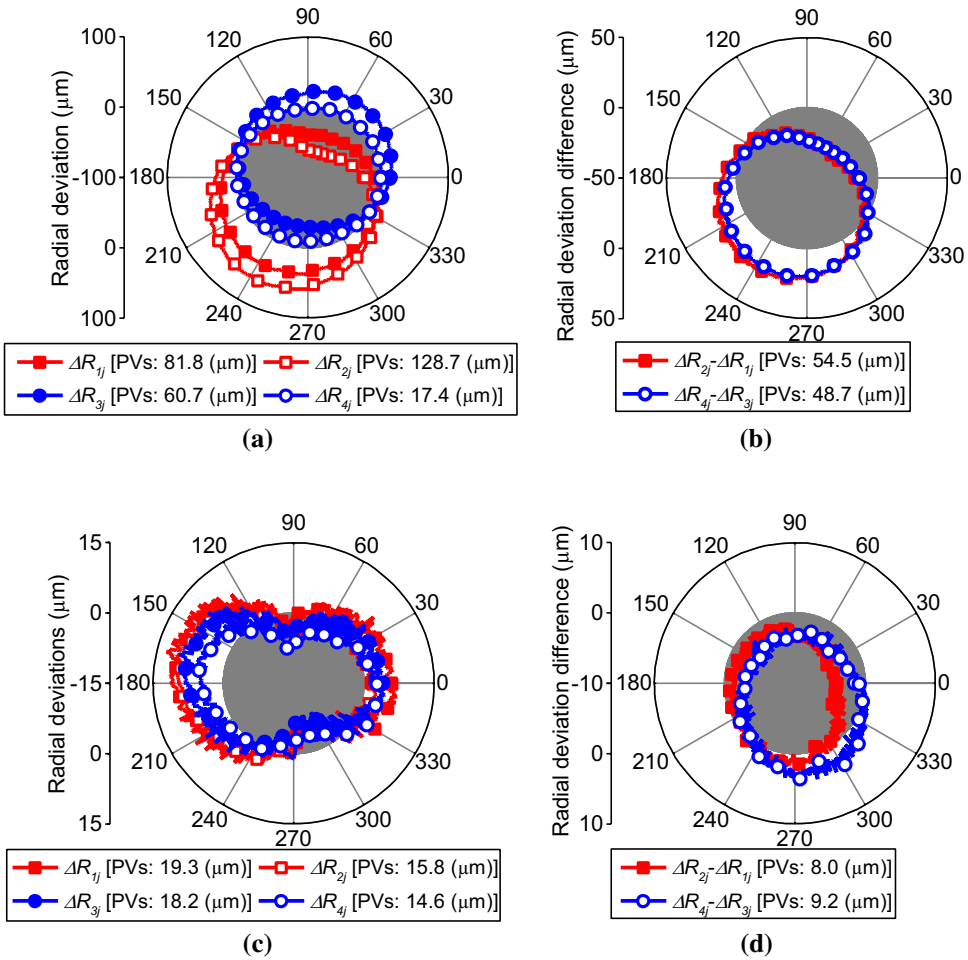

Fig. 5 Measured radial deviations and differences used for identification of parallelism errors. **a** Without compensation. **b** Differences without compensation. **c** With compensation. **d** Differences with compensation

significantly after compensation for the parallelism errors which were identified successfully by our method.

3.2 Verification of the Identified Parallelism Errors

It is essential to check the validity of identified parallelism errors to improve machining accuracy. Thus, we sequentially machined the concentric $hole_s$ and $hole_l$ using a short and long tool, respectively (Fig. 6a, b), because parallelism errors affect tools of different lengths differently, in turn influencing hole positional deviations and concentricity. The experimental conditions are summarized in Table 2.

The holes were machined without and with tool-center-point compensation for the identified parallelism errors of three samples. The machined holes were measured using a coordinate measuring machine (Fig. 6c). Without compensation, large positional deviations and poor concentricity were evident, attributable largely to parallelism errors (Fig. 6d). The average positional deviations of $hole_l$ relative to the center of $hole_s$ were $(-5.8, -30.7)$ and $(-1.4, -15.9)$ μm without and with compensation, respectively. In terms of concentricity, the distances between the centers of $hole_s$ and $hole_l$ were 31.2 and 15.9 μm, respectively. Note that both positional deviations and concentricity improved considerably, although they remain affected by the Z-axis PDGEs. Our method was effective.

4 Conclusions

We derived the inherent spindle axis parallelism errors of machine tools. Our dual difference method features two pairs of circular tests using a DBB; we optimized the test using the RSS values of the sensitivity coefficients. These accurately identify errors imparted by the kinematic structure of experimental machine tools. Identification and compensation of parallelism errors using the dual difference method will improve the volumetric accuracies of machine tools. Our principal findings are as follows.

(1) The linearized relationships among radial deviations, geometric errors, and set-up errors yield critical information when identifying inherent parallelism errors. Such errors affect the radial deviations coupled with other errors. Parallelism errors can be identified by pre-

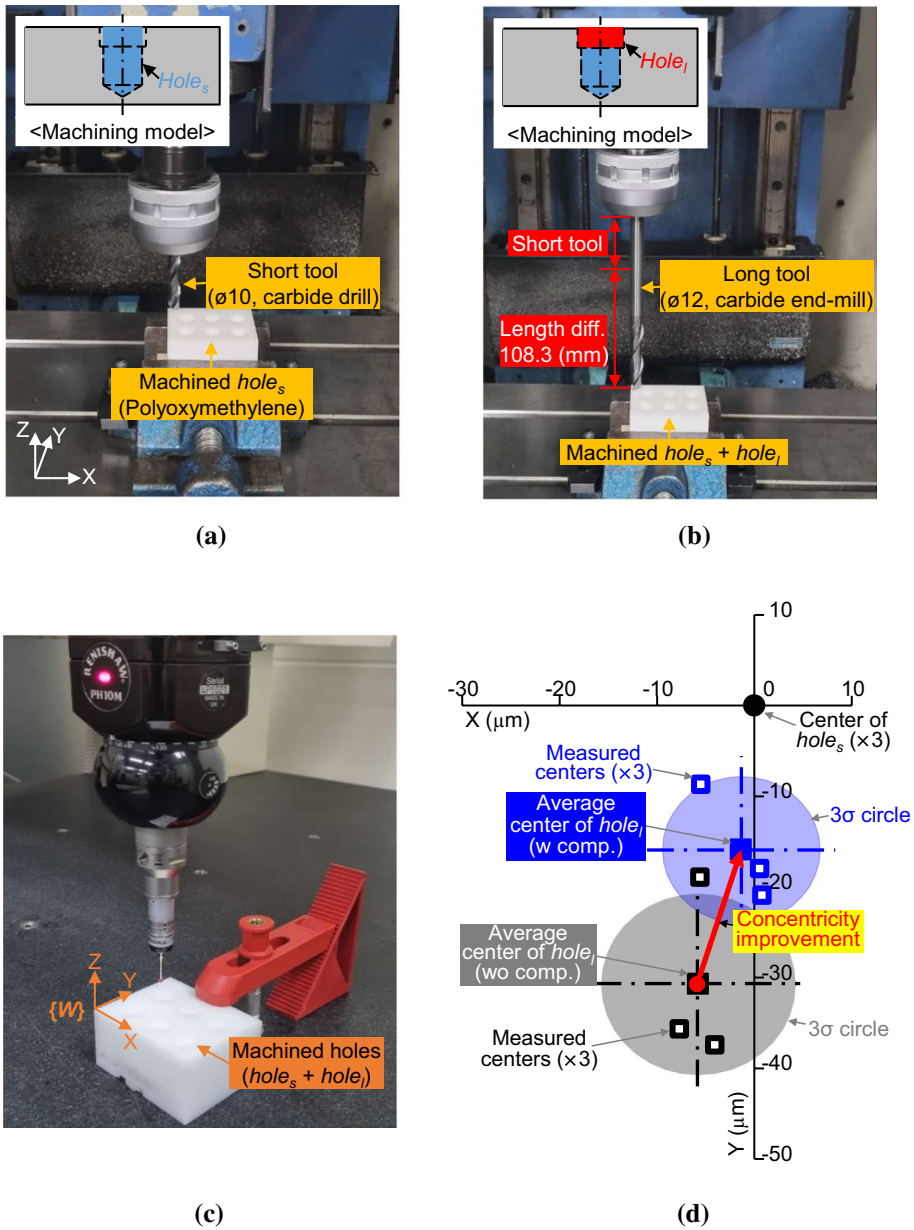

Fig. 6 Machining tests on concentric holes and concentricity measurements. **a** $Hole_s$ was drilled using a short tool. **b** $Hole_l$ drilled using a long tool. **c** Measurements of machined holes derived using a CMM. **d** Measured centers of $hole_s$ and $hole_l$, with concentricity improvement after compensation

measuring the other errors and incorporating them into the relationships. However, it is difficult to quantify set-up errors attributable to (largely unknown) geometric errors. Therefore, it is essential to use differences between circular tests to cancel the effects of set-up errors on parallelism errors.

(2) A dual difference method appropriately identifies inherent spindle axis parallelism errors (unaffected by geometric errors of linear axes or by set-up errors), based on DBB measurements. Within each pair, circular tests using different tool lengths were performed at the first and last points of the Z-axis, using a shared set-up that canceled the X- and Y-axis PDGEs and set-up errors. Data from the two pairs showed inherent parallelism errors relative to the end-point reference straight line of the Z-axis, by canceling the Z-axis PDGEs using the difference of the differences (the dual difference).

(3) Three offsets are required when performing the two pairs of circular tests that identify parallelism errors using a dual difference method. The distance between the spindle tip and workpiece table of a machine tool affects the DBB offsets. One offset should equal the minimum Z-axis value of the end-point reference straight line; the other offsets are determined by mini-

Table 2 Experimental conditions for parallelism error verification

Item		Specification
Tool	For $hole_s$	DPPA01100 (YG-1 Co. Ltd, Republic of Korea), ø10 carbide drill
	For $hole_l$	VAC-PEM2EXL12-60–200 (MISUMI Co., Japan), ø12 carbide end-mill
	Length difference between tools, mm	108.3
Workpiece	Material	Polyoxymethylene
Hole size	For $hole_s$, mm	ø10 × 10
	For $hole_l$, mm	ø10 × 10
Machining condition	Feedrate, mm/min	10
	Spindle speed, rpm	3,000

mizing the RSSs of the sensitivity coefficients, reducing measurement uncertainties even if the contributors thereto are imperfect.

(4) The dual difference method is not only limited to use of a DBB but also the use of a linear displacement sensor and test spheres (not a sphere in ISO 230–1:2012), or a dial gauge and test mandrels (not a mandrel in ISO 10791–1:2015). However, use of a DBB is advantageous because of the simple measuring processes, using commercial products supporting automated data acquisition, averaging effects and improved measurement uncertainties by large sampling numbers at each circular test.

The dual difference method is not limited to three-axis machine tools; it is also applicable to five-axis machine tools featuring two workpiece rotary axes, two spindle head rotary axes, and a swivel head and/or a rotary table. In the last two cases, squareness errors (not parallelism errors) are used to describe the spindle axis relative to the rotary axis head. Squareness errors can be identified using a dual difference method because the method considers the spindle axis relative to the Z-axis.

Acknowledgements This work was supported by the National Research Foundation of Korea (NRF) grant funded by the Korea government (MSIT) (Nos. 2020R1C1C100330011, 2019R1A2C2088683).

Funding This work was supported by the National Research Foundation of Korea(NRF) grant funded by the Korea government(MSIT) (No. 2020R1C1C100330011, 2019R1A2C2088683).

Declarations

Conflict of interest The authors declare that they have no conflict of interest.

References

1. Yang, S. H., & Lee, K. I. (2021). Machine tool analyzer: A device for identifying 13 position–independent geometric errors for five–axis machine tools. *The International Journal of Advanced Manufacturing Technology, 115*, 2945–2957. https://doi.org/10.1007/s00170-021-07341-7
2. Lee, K. I., & Yang, S. H. (2013). Measurement and verification of position–independent geometric errors of a five–axis machine tool using a double ball–bar. *International Journal of Machine Tools and Manufacture, 70*, 45–52. https://doi.org/10.1016/j.ijmachtools.2013.03.010
3. ISO 230–1. (2012). Test code for machine tools – Part 1: Geometric accuracy of machines operating under no–load or quasi–static conditions. *ISO*.
4. ISO 230–7. (2015). Test code for machine tools – part 7: Geometric accuracy of axes of rotation. *ISO*.
5. Schwenke, H., Knapp, W., Haitjema, H., Weckenmann, A., Schmitt, R., & Delbressine, F. (2008). Geometric error measurement and compensation of machines–An update. *CIRP Annals, 57*, 660–675. https://doi.org/10.1016/j.cirp.2008.09.008
6. Ibaraki, S. & Knapp, W. (2012). Indirect measurement of volumetric accuracy for three–axis and five–axis machine tools: A review. *International Journal of Automation Technology*, 6: 110–124. https://doi.org/10.20965/ijat.2012.p0110
7. ISO 230–2. (2014). Test code for machine tools – part 2: Determination of accuracy and repeatability of positioning of numerically controlled axes. *ISO*.
8. Liu, H., Yang, R., Wang, P., Chen, J., Xiang, H., & Chen, G. (2020). Measurement point selection and compensation of geometric error of NC machine tools. *The International Journal of Advanced Manufacturing Technology, 108*, 3537–3546. https://doi.org/10.1007/s00170-020-05411-w
9. Wang, Z., Wang, D., Wu, Y., Dong, H., & Yu, S. (2021). An invariant approach replacing Abbe principle for motion accuracy test and motion error identification of linear axes. *International Journal of Machine Tools and Manufacture, 166*, 103746. https://doi.org/10.1016/j.ijmachtools.2021.103746
10. ISO 230–4. (2005). Test code for machine tools part 4: Circular tests for numerically controlled machine tools. *ISO*.
11. Wang, Z., Wang, D., Yu, S., Li, X., & Dong, H. (2021). A reconfigurable mechanism model for error identification in the double ball bar tests of machine tools. *International Journal of Machine Tools and Manufacture, 165*, 103737. https://doi.org/10.1016/j.ijmachtools.2021.103737
12. ISO 203–6. (2002). Test code for machine tools – part 6: Determination of positioning accuracy on body and face diagonals (diagonal displacement tests). *ISO*.
13. Yang, S. H., Lee, H. H., & Lee, K. I. (2019). Identification of inherent position-independent geometric errors for three-axis machine tools using a double ballbar with an extension fixture. *The International Journal of Advanced Manufacturing Technology, 102*, 2967–2976. https://doi.org/10.1007/s00170-019-03409-7
14. ISO/TR 230–11. (2018). Test code for machine tools – part 11: Measuring instruments suitable for machine tool geometry tests. *ISO*.

15. ISO 10791–1. (2015). Test conditions for machining centres part 1: Geometric tests for machines with horizontal spindle (horizontal Z-axis). *ISO*.
16. ISO 10791–2. (2001). Test conditions for machining centres part 2: Geometric tests for machines with vertical spindle or universal heads with vertical primary rotary axis. *ISO*.
17. Lee, K. I., Shin, D. H., & Yang, S. H. (2017). Parallelism error measurement for the spindle axis of machine tools by two circular tests with different tool lengths. *The International Journal of Advanced Manufacturing Technology, 88*, 2883–2887. https://doi.org/10.1007/s00170-016-8999-0
18. Yang, S. H., Lee, D. M., Lee, H. H., & Lee, K. I. (2020). Sequential measurement of position-independent geometric errors in the rotary and spindle axes of a hybrid parallel kinematic machine. *International Journal of Precision Engineering and Manufacturing, 21*, 2391–2398. https://doi.org/10.1007/s12541-020-00437-2
19. Dassanayake, K. M. M., Tsutsumi, M., & Saito, A. (2006). A strategy for identifying static deviations in universal spindle head type multi-axis machining centers. *International Journal of Machine Tools and Manufacture, 46*, 1097–1106. https://doi.org/10.1016/j.ijmachtools.2005.08.010
20. ISO/IEC Guide 98–3. (2008). Uncertainty of measurement – part 3: Guide to the expression of uncertainty in measurement (GUM:1995). *ISO*.
21. ISO 230–9. (2005). Test code for machine tools – part 9: Estimation of measurement uncertainty for machine tool tests according to series iso 230, basic equations. *ISO*.
22. Ibaraki, S., & Hiruya, M. (2021). A novel scheme to measure 2D error motions of linear axes by regulating the direction of a laser interferometer. *Precision Engineering, 67*, 152–159. https://doi.org/10.1016/j.precisioneng.2020.09.011
23. Yang, S. H., & Lee, K. I. (2021). Identification of 11 position–independent geometric errors of a five–axis machine tool using 3D geometric sensitivity analysis. *The International Journal of Advanced Manufacturing Technology, 113*, 3271–3282. https://doi.org/10.1007/s00170-021-06844-7
24. Lee, D. M., & Yang, S. H. (2010). Mathematical approach and general formulation for error synthesis modeling of multi-axis system. *International Journal of Modern Physics B, 24*, 2737–2742. https://doi.org/10.1142/S0217979210065556
25. Lee, K. I., & Yang, S. H. (2013). Robust measurement method and uncertainty analysis for position-independent geometric errors of a rotary axis using a double ball-bar. *International Journal of Precision Engineering and Manufacturing, 14*, 231–239. https://doi.org/10.1007/s12541-013-0032-z

Seung-Han Yang received a Ph.D. degree in Mechanical Engineering from the University of Michigan, Ann Arbor, Michigan, USA. He is currently a professor in the School of Mechanical Engineering, Kyungpook National University. His research interest is intelligent manufacturing systems and CAD/CAM.

Kwang-Il Lee received a Ph.D. degree in Mechanical Engineering from Kyungpook National University, Daegu, Republic of Korea. He is currently a professor in the School of Mechanical and Automotive Engineering, Kyungil University. His research interest is precision methodologies for machine tools, precision robots, and 3D printers.